J Physiol 587.18 (2009) pp 4523–4541

The Journal of Physiology

The Q_γ component of intra-membrane charge movement is present in mammalian muscle fibres, but suppressed in the absence of S100A1

Benjamin L. Prosser[1], Erick O. Hernández-Ochoa[1], Danna B. Zimmer[2] and Martin F. Schneider[1]

[1]*Department of Biochemistry and Molecular Biology, University of Maryland School of Medicine, 108 N. Greene Street, Baltimore, MD 21201, USA*
[2]*Department of Veterinary Pathobiology, College of Veterinary Medicine, Texas A&M University, College Station, TX 77843-4467, USA*

S100A1 is a Ca^{2+} binding protein that modulates excitation–contraction (EC) coupling in skeletal and cardiac muscle. S100A1 competes with calmodulin for binding to the skeletal muscle SR Ca^{2+} release channel (the ryanodine receptor type 1, RyR1) at a site that also interacts with the C-terminal tail of the voltage sensor of EC coupling, the dihydropyridine receptor. Ablation of S100A1 leads to delayed and decreased action potential evoked Ca^{2+} transients, possibly linked to altered voltage sensor activation. Here we investigate the effects of S100A1 on voltage sensor activation in skeletal muscle utilizing whole-cell patch clamp electrophysiology to record intra-membrane charge movement currents in isolated flexor digitorum brevis (FDB) muscle fibres from wild-type and S100A1 knock-out (KO) mice. In contrast to recent reports, we found that FDB fibres exhibit two distinct components of intra-membrane charge movement, an initial rapid component (Q_β), and a delayed, steeply voltage dependent 'hump' component (Q_γ) previously recorded primarily in amphibian but not mammalian fibres. Surprisingly, we found that Q_γ was selectively suppressed in S100A1 KO fibres, while the Q_β component of charge movement was unaffected. This result was specific to S100A1 and not a compensatory result of genetic manipulation, as transient intracellular application of S100A1 restored Q_γ. Furthermore, we found that exposure to the RyR1 inhibitor dantrolene suppressed a similar component of charge movement in FDB fibres. These results shed light on voltage sensor activation in mammalian muscle, and support S100A1 as a positive regulator of the voltage sensor and Ca^{2+} release channel in skeletal muscle EC coupling.

(Resubmitted 22 June 2009; accepted after revision 31 July 2009; first published online 3 August 2009)
Corresponding author M. F. Schneider: 108 N. Greene Street, Baltimore, MD 21201, USA.
Email: mschneid@umaryland.edu

Abbreviations CaM, calmodulin; CaMBD, calmodulin binding domain; DHPR, dihydropyridine receptor; EDL, extensor digitorum longus; FDB, flexor digitorum brevis; KO, knock out; RyR, ryanodine receptor; SR, sarcoplasmic reticulum.

Skeletal muscle excitation–contraction (EC) coupling is the process by which membrane depolarization triggers sarcoplasmic reticulum (SR) Ca^{2+} release and subsequent contractile activation. Depolarization of the transverse (T) tubule system is detected by the voltage sensor of EC coupling, the dihydropyridine receptor (DHPR), an L-type Ca^{2+} channel ($Ca_V1.1$). Upon depolarization there is a reorientation of positively charged residues in the transmembrane domain of DHPR that triggers Ca^{2+} release from the coupled ryanodine receptor (RyR1) in the SR membrane (Schneider & Chandler, 1973; Horowicz & Schneider, 1981*b*; Huang, 1988; Ríos & Pizarro, 1991).

RyR-mediated Ca^{2+} release is modulated by Ca^{2+} and Mg^{2+}, as well as by endogenous proteins such as FKBP12, calmodulin, calsequestrin and, more recently, S100A1 (Tripathy *et al.* 1995; Ikemoto *et al.* 1989; Jayaraman *et al.* 1992; Meissner, 1994; Treves *et al.* 1997). S100A1 is a small Ca^{2+} binding protein highly expressed in striated muscle and localized to the Ca^{2+} release units of skeletal and cardiac muscle cells (Haimoto & Kato, 1987; Zimmer *et al.* 1991; Most *et al.* 2003; Prosser *et al.* 2007). S100A1 interacts with both skeletal and cardiac RyR isoforms and enhances SR Ca^{2+} release. In the heart, S100A1 improves Ca^{2+} cycling and contractile performance (for a

B. L. Prosser and E. O. Hernández-Ochoa contributed equally to this work.

DOI: 10.1113/jphysiol.2009.177238

detailed review see Most *et al.* 2007), and is being rapidly pursued as a gene therapeutic agent for the treatment of cardiomyopathy (Pleger *et al.* 2007; Vinge *et al.* 2008). The ablation of S100A1 results in ventricular conduction defects and increased mortality following myocardial infarction (Ackermann *et al.* 2008; Desjardins *et al.* 2009). While skeletal muscle research has been less extensive, several groups have demonstrated direct effects of S100A1 on skeletal muscle EC coupling. Specifically, S100A1 binds to RyR1 with nanomolar affinity and increases the open probability of the channel (Treves *et al.* 1997), and exogenous S100A1 enhances Ca^{2+} release and force in skinned slow and fast twitch muscle fibres (Most *et al.* 2003). We recently have shown that S100A1 competes with calmodulin (CaM) for the CaM binding site on RyR1, and have mapped this interaction using NMR spectroscopy (Prosser *et al.* 2007; Wright *et al.* 2008). Furthermore, we showed that compared to muscle fibres from wild-type (WT) animals, muscle fibres from an S100A1 knock-out (KO) animal demonstrate smaller and more slowly developing Ca^{2+} transients when stimulated with an action potential, which can be reversed with adenoviral delivery of S100A1 (Prosser *et al.* 2007).

Enhancement of SR Ca^{2+} release could be the result of a direct interaction between S100A1 and RyR1, as supported by studies with the purified channel (Treves *et al.* 1997). A second, not mutually exclusive possibility is that modulation of the voltage sensor mediates S100A1's effect on Ca^{2+} release. This hypothesis is supported by the following. (1) S100A1 modulates the DHPR L-type Ca^{2+} channel in cardiomyocytes (Reppel *et al.* 2005). (2) S100A1 binds to the CaM binding site on RyR1 (Prosser *et al.* 2007; Wright *et al.* 2008), a site proposed to bind and stabilize the C-terminal tail of the DHPR (Sencer *et al.* 2001). (3) S100A1 binds RyR1 and enhances Ca^{2+} signalling, which may contribute to bi-directional crosstalk between RyR1 and DHPR, a previously documented pathway (Nakai *et al.* 1996; Avila & Dirksen, 2000). For these reasons we sought to explore the effect of S100A1 on the activation of the voltage sensor of EC coupling.

A classical approach to studying DHPR activation in skeletal muscle is to record gating currents elicited by sarcolemmal and transverse tubule depolarization. This is performed by eliminating ionic and linear capacitive currents, thereby allowing the isolation of non-linear capacitive currents arising primarily from the movement of intra-membrane charged residues in the DHPR (Schneider & Chandler, 1973; Chandler *et al.* 1976). Initial studies in frog muscle showed that a certain amount of charge must be moved to trigger Ca^{2+} release and fibre contraction (Kovacs *et al.* 1979; Horowicz & Schneider, 1981*a*). Since then, recording of charge movement has been used extensively to study DHPR mediated activation of Ca^{2+} release in skeletal muscle, at first largely in amphibian muscle (Hui, 1983; Pizarro *et al.* 1989; Csernoch *et al.* 1991; García *et al.* 1991), and more recently in mammalian muscle (Wang *et al.* 1999; Avila & Dirksen, 2000; Royer *et al.* 2008). Here we utilize whole-cell patch clamp electrophysiology to record charge movement currents in mammalian skeletal muscle fibres from WT and S100A1 KO animals. We show that WT mammalian fibres exhibit two components of charge movement, including a temporally delayed, steeply voltage-dependent component reminiscent of 'Q_γ' previously identified in amphibian muscle fibres (Adrian & Almers, 1976; Adrian & Peres, 1977). We also demonstrate for the first time that the absence of an endogenous protein can markedly affect voltage sensor charge movement, as Q_γ is suppressed in fibres lacking S100A1. Furthermore, we show that Q_γ can be restored in KO fibres by transient application of S100A1, and is at least partially suppressed by the RyR1 inhibitor dantrolene. These results shed light on the nature of voltage sensor charge movement in mammalian muscle, as well as furthering our understanding of S100A1's modulation of EC coupling. A detailed examination of the relationship between voltage sensor charge movement and RyR Ca^{2+} release in both wild-type and S100A1 deficient muscle fibres is provided in a companion paper.

Methods

Ethical approval

All animals were housed in a pathogen-free area at the University of Maryland, Baltimore. The animals were killed according to authorized procedures of the Institutional Animal Care and Use Committee, University of Maryland, Baltimore (Baltimore, MD), by regulated delivery of compressed CO_2 overdose followed by decapitation.

FDB fibre preparation

Fibres were prepared using enzymatic dissociation of FDB muscles of 6- to 7-week-old C57 × 129 WT and S100A1 KO mice, and were cultured as previously described (Liu *et al.* 1997). $S100A1^{-/-}$ animals and WT littermate control animals were obtained from Dr Danna Zimmer, Texas A&M University. The generation and genotyping of these animals has been previously reported (Prosser *et al.* 2007).

Solutions

For whole-cell Ca^{2+} current measurements bath (external) solution contained (in mM): 150 TEA-CH_3SO_3, 2 $CaCl_2$, 10 Hepes, 1 $MgCl_2$, 0.001 TTX, 1 4-aminopiridine, 0.025 *N*-benzyl-*p*-toluene sulphonamide (BTS), pH adjusted to 7.4 with CsOH. For non-linear capacitive current recording we use a similar external solution, except we

added 0.5 $CdCl_2$ and 0.5 $CoCl_2$, and $CaCl_2$ was reduced to 1 to keep the total divalent concentration constant.

The standard pipette solution (internal solution) contained (in mM): 140 Cs-CH_3SO_3, 10 Hepes, 20 EGTA, 4 $MgCl_2$, 4 Na_2ATP, 14 creatine PO_4, 0.3 Na_2GTP and 0.1 leupeptin, pH adjusted to 7.4 with CsOH. The choice of such solution was the result of a large series of trial and error tests in preliminary experiments. Compared with large non-permeable inorganic (NMG^+ and TEA^+) or organic (aspartate and glutamate) cations, we obtained with a Cs^+-based solution a large improvement in sealing, durability, blocking of ionic currents, and comparability with experiments at the level of ionic current.

Alexa-Fluor-488 labelled S100A1 protein was a generous gift from Drs Nathan Wright and David Weber, University of Maryland, Baltimore.

Electrophysiology and data analysis

Membrane current measurements were performed using the whole-cell configuration of the patch-clamp technique (Hamill *et al.* 1981) as previously detailed by Wang *et al*. (1999) for mammalian FDB fibres but with some modifications. We use an EPC-10 (HEKA Instruments Inc., Bellmore, NY, USA) amplifier and Parafilm coated pipettes of borosilicate glass (WPI-TW150F3) with resistance of 1.2–1.6 MΩ when filled with the internal solution. Once the whole-cell configuration was established, cells were held at −60 mV and the capacitance compensation partially adjusted. Series resistance was compensated to 50–65%. Fibres with signs of qualitative clamp error, such as unstable series resistance, unstable holding current, or a stable holding current above 8 nA, were rejected from the analysis. Measurements were started 20 min after whole-cell configuration was established.

Voltage protocols were generated and current responses were digitized and stored using Patchmaster and Fitmaster (HEKA Instruments). Command pulses were delivered at 10 s intervals to the levels and duration indicated in each figure from a holding potential of −80 mV, unless otherwise indicated. Currents were typically low-pass-filtered at 3–10 kHz (3-pole Bessel filter). Currents were sampled at 10 kHz. Linear capacitive and ionic currents were routinely subtracted by a *P*/4 protocol from a subholding potential of −20 mV. Gating charge moved during each test depolarization (Q_{ON}) was quantified by calculating the area under the curve of each trace of non-linear current using the post-transient level of each trace as a steady-state value of non-linear ionic current. Total charge moved during repolarization (Q_{OFF}) was calculated similarly. Total charge movement was normalized to the linear fibre capacitance, which was estimated using the following equation: $C = Q/V$. C was determined by measuring linear capacitive current elicited by a ±5 mV test pulse from the holding potential and integrating the area under the capacitive current trace to estimate Q.

Temporal differences in charge development at different voltage steps and between WT and KO groups were considered in setting the time to integrate during a typical 80 ms pulse. To minimize ionic contamination of the ON current, the time of integration for Q_{ON} was set to the nearest approximation of the end of Q development. As such, for steps to −70 through −40 mV, and for steps above 0 mV, the time of integration for the ON current was set between 15 and 25 ms. For steps to −30 through 0 mV, the time of integration was increased to between 25 and 35 ms due to the presence of a temporally delayed component in WT fibres. In KO fibres lacking a temporally delayed component, an increase in integration time was not required. As a visual depiction of these different integration time points, hash marks have been included on the ON current traces in Fig. 1*C* to mark the end of the integration time. The time of integration for the OFF current was always set to 50 ms after the pulse. Quantification of charge movement will be considered further in the results.

Western blotting

Western blots were performed as in Liu *et al.* (2009) with modifications. Tibialis anterior muscles were isolated from WT and S100A1$^{-/-}$ animals, frozen in liquid nitrogen, and stored at −80°C. Muscles were ground to a fine powder at −20°C with mortar and pestle, then lysed and centrifuged, and the soluble fraction collected as previously described (Liu *et al.* 2009). Protein content was determined using the Bradford assay (Bio-Rad, Hercules, CA, USA). Approximately 50 μg of protein from each sample was separated by SDS-PAGE using a 4–12% gradient gel and transferred to PVDF membrane. Blots were then processed and probed with the appropriate antibodies. The antibody for DHPR α_1s was purchased as tissue culture supernatant from Developmental Studies Hybridoma Bank (Iowa City, IA, USA) and used at a 1 : 100 dilution. The antibody for glyceraldehyde phosphate dehydrogenase (GAPDH) was from Sigma (St Louis, MO, USA). Immunoreactive bands were visualized by ECL Western Blotting Detection Reagents (GE Healthcare (Amersham), Piscataway, NJ, USA).

Fluo-4AM Ca^{2+} transient recordings

Action potential evoked Ca^{2+} transients were monitored using the fluorescent indicator Fluo-4AM and ultra high-speed confocal microscopy (Zeiss LSM 5 LIVE system) as previously described (Prosser *et al.* 2007).

Statistical analysis

All statistical analysis was performed using OriginPro8.0 (OriginLab Corp., Northampton, MA, USA). All data are presented as mean values ± standard error of the mean (S.E.M.) unless otherwise noted. Normality of data sets was ensured for each statistical calculation. Significance was determined using Student's *t*-test and set at $P < 0.05$.

Results

Non-linear charge movement currents are different in WT and S100A1 KO fibres

Figure 1 presents non-linear capacitive current records obtained from a FDB fibre from an S100A1 KO mouse (Fig. 1*B*) and from a WT littermate (Fig. 1*A*). The current components were elicited with 80 ms depolarizing test pulses to voltages ranging from −70 to +20 mV in 10 mV increments. The displayed records are typical of those obtained from 11 fibres from KO mice and 12 fibres from WT littermates. The transient positive (outward) non-linear current at the start of each depolarization was primarily due to outward movement of intramembrane charged voltage sensors. The more slowly developing or maintained inward or outward current following the transient charge movement current during the larger pulses represents slowly developing or constant voltage-dependent ionic current. The transient negative (inward) current at the end of the pulse was primarily due to the return of these mobile intramembrane charges

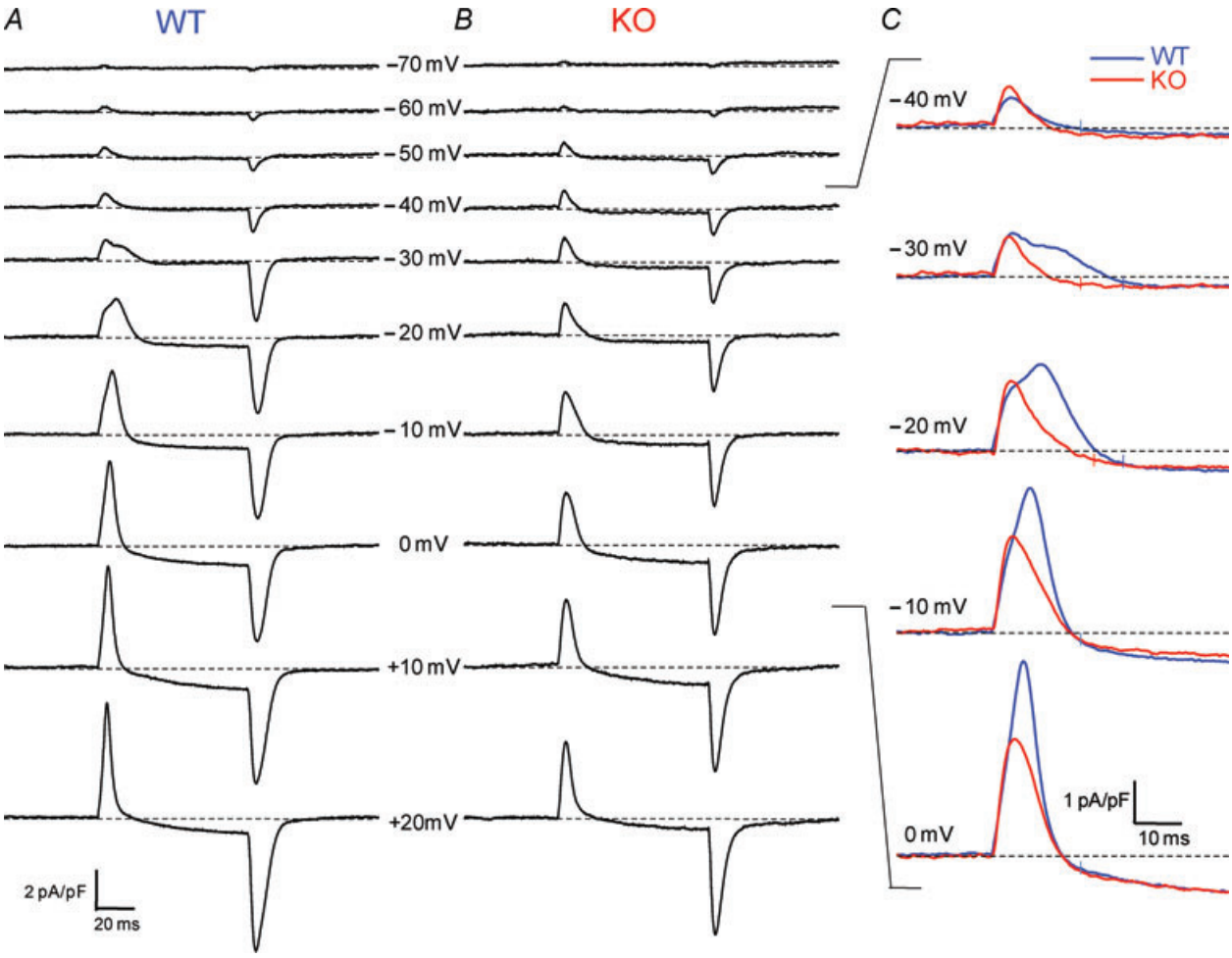

Figure 1. Whole-cell patch clamp recordings of non-linear capacitive (charge movement) currents in WT and KO FDB fibres
A and *B*, representative charge movement current traces elicited by 80 ms depolarizing steps from a holding potential of −80 mV. In all traces dotted line represents the zero baseline. *C*, zoom in of the ON current of superimposed WT and KO current traces demonstrates suppression of temporally delayed 'hump' component (Q_γ) in KO fibres. Typically WT fibres developed a noticeable hump around −20 mV, whereas no distinct second component was seen in KO fibres. Colour-coordinated hash marks on current traces represent integration times to establish '*Q*' for WT and KO fibres, set to 20, 25, or 30 ms depending on the appearance of a temporally delayed component. A single hash mark implies that the same time to integration was used for both traces.

when the membrane potential was restored to the holding voltage, with a possible additional contribution from non-linear tail currents flowing through ion channels activated during the depolarization. Ionic current interference with the charge movement currents was typically minimal for depolarizations to voltages ranging from −70 to −10 mV, but became increasingly important for larger depolarizations. Procedures for minimizing the influence of such ionic current components on charge movement characterization and quantification will be presented in the following section.

Simple visual comparison of the representative non-linear current records in Fig. 1 reveals several similarities and differences between charge movement currents recorded from the KO and WT fibres. (1) For depolarizations to −70 to −40 mV, the amplitude of the transient currents and their relatively simple time course were similar for KO and WT fibres. (2) During pulses to −30 to 0 mV the charge movement records from the WT fibres exhibited a temporally delayed 'hump' component after the initial peak, whereas KO fibres continued to display a time course consisting of a relatively rapid rise followed by a simple decay (see superimposed records in Fig. 1*C*). A temporally delayed component of charge movement that arises at intermediate depolarizations and produces a 'hump' in non-linear current records has been previously described in amphibian fibres and termed Q_γ (Adrian & Almers, 1976; Adrian & Peres, 1977). We will adapt this terminology for the temporally delayed component seen in mammalian fibres here. Due to the similar initial phase in WT and KO fibres, but the presence of a delayed extra component only in the WT fibre, the charge moved by the charge movement current became larger for the WT than for the KO fibre over this intermediate voltage range. (3) For even larger depolarizations (to +10 and +20 mV), a kinetically delayed component was no longer obviously distinguishable. However, the amplitude of the transient charge movement current (and its area) continued to be larger for the WT than for the KO fibre, indicating greater charge moved in the WT fibre. These observations were generally characteristic of WT and KO fibres studied.

Isolation, verification and quantification of charge movement currents

Before quantifying the observations in the preceding paragraph, it is important to establish measures of charge movement that are not appreciably contaminated by non-linear ionic current contributions. The successful elimination of ionic current results in a charge movement current that saturates at extreme voltages, and demonstrates an equal amount of charge moved during depolarization (Q_{ON}) and repolarization (Q_{OFF}). As seen in Fig. 2*B*, Q_{ON} and Q_{OFF} demonstrated ON/OFF equality with minimal ionic contamination during and after 80 ms steps to −70 mV to −10 mV (Fig. 2*A*, top and 2*B*). However, Q_{OFF} became significantly larger than Q_{ON} after 80 ms steps to 0 mV and more positive voltages, suggesting ionic contamination of the OFF recordings, as can be visualized with the longer depolarizing step in Fig. 2*A*, bottom. To minimize possible non-linear ionic current contamination of the OFF current, we used shorter, 25 ms steps to 0, +10 and +20 mV. This step was of adequate duration to achieve complete charge movement at these voltages, and minimizes the ionic contamination of the OFF, as seen in the ON/OFF equality of the open and filled circles in Fig. 2*B* and with the shorter depolarizing step in Fig. 2*A*, bottom. For approximately half the fibres tested we also used 25 ms steps to +30 mV and +40 mV, and found that despite increasing ionic contamination, ON and OFF charge movement were completely saturated at these voltages. These short steps could not be used for the less depolarized voltages, as fibres that exhibited a temporally delayed component elicited charge movement currents lasting longer than 25 ms (demonstrated in Fig. 1*C*). Ionic contamination of the ON current also appears to have led to a slight underestimation of charge moved at the most positive steps. For this and the other reasons detailed above, to achieve our measure of charge movement (Q) we integrated the ON current traces for 80 ms steps from −70 to −10 mV, and averaged the ON and OFF integrations from short 25 ms pulses for steps from 0 to +20 mV. Following these parameters fibres demonstrated ON/OFF equality, as demonstrated by the linear relationship between the ON and OFF charge seen in Fig. 2*C*.

As the *P*/4 protocol was used to subtract linear capacitive currents and isolate non-linear charge movement currents during depolarizing pulses, we sought to ensure linearity of membrane properties over the voltage range used to obtain these subtraction templates. Figure 2*D* demonstrates a sum response (black trace) to opposite polarity 20 mV voltage steps from a holding potential of −120 mV. The red and grey traces represent the total current from the depolarizing and hyperpolarizing steps, respectively. As can be seen the sum of these two currents is essentially zero, suggesting linearity of membrane currents at these very negative potentials. Figure 2*E* shows the remaining non-linear current elicited by an 80 mV step to 0 mV in a representative WT fibre (blue trace), after subtraction with the *P*/4 protocol. Below is the amplitude of the subtraction template (middle current trace) and the template scaled up by a factor of 4 (bottom current trace), as would be used in the subtraction from an 80 mV step. Remaining non-linear currents in the control pulses appear negligible compared to the relatively large charge movement currents, validating the use of this technique to isolate non-linear capacitive currents in FDB fibres.

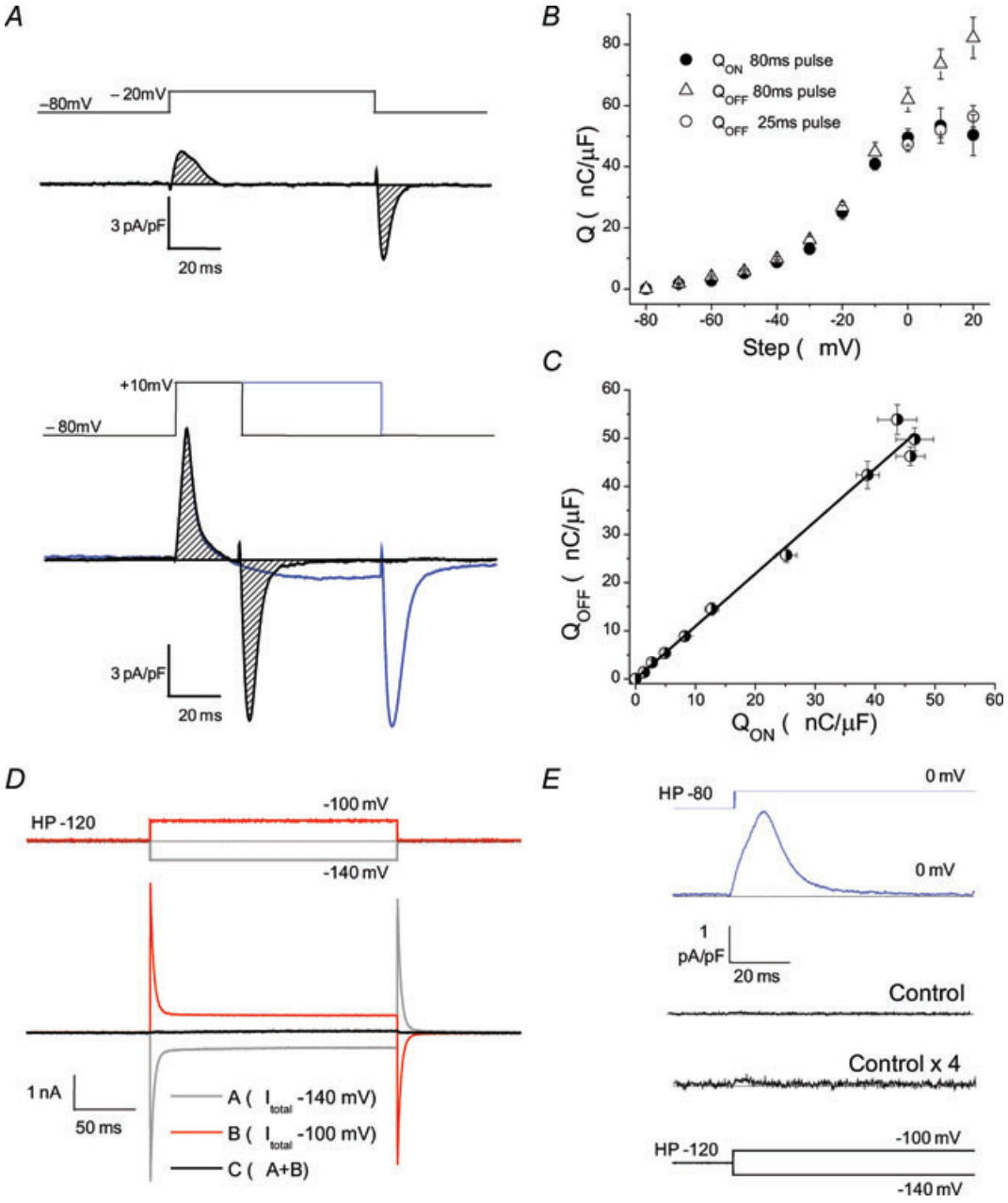

Figure 2. Quantification of charge movement recordings
A, top, charge movement current trace elicited by an 80 ms step to −20 mV demonstrates ON/OFF conservation with minimal ionic interference. Shaded region marks the area of integration to establish Q_{ON} and Q_{OFF}, which are quantified in Fig. 2*B*. Bottom, at steeper depolarizing, 80 ms steps (such as to +10 mV, blue trace) significant ionic contamination leads to an overestimation of Q_{OFF}, as seen by the open triangles in Fig. 2*B*. For this purpose we used shorter, 25 ms steps (black trace) to minimize ionic contamination. Integrating these ON and OFF currents from shorter steps showed charge conservation, quantified with the open and filled circles in Fig. 2*B*. *B*, Q_{ON} and Q_{OFF} *vs.* voltage relationship in WT fibres. Filled circles are Q_{ON} established by integrating non-linear current traces during an 80 ms pulse. Open triangles are Q_{OFF} from the same 80 ms pulse; note overestimation of Q_{OFF} at steeper depolarizations, a clear indication of ionic contamination of the OFF records. Open circles are Q_{OFF} during a 25 ms pulse. Based on the above we averaged Q_{ON} and Q_{OFF} from a 25 ms pulse to establish '*Q*' at steeper depolarizations. *C*, Q_{ON} *vs.* Q_{OFF} relationship demonstrates charge conservation when using above criteria, using Q_{ON} values from 80 ms pulses, and Q_{OFF} values from 80 ms pulses for steps to −80 through −10 mV and from 25 ms pulses for steps to 0 through +20 mV. The data were fitted with a linear function with a slope of 1.09 and $R^2 = 0.986$. *D*, sum response (black) to opposite polarity 20 mV voltage steps (red and grey traces) from a holding

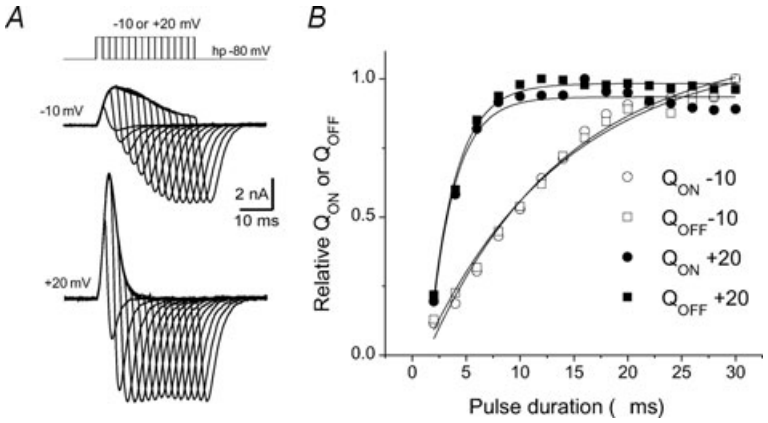

Figure 3. Charge conservation
A, charge movement currents recorded in response to depolarizing pulses to −10 and +20 mV of increasing duration (2 ms increments) to evaluate charge movement conservation. *B*, Q_{ON} or Q_{OFF} *vs.* pulse duration for the complete set of pulses of corresponding traces illustrated in *A*. The normalized charge-pulse duration relationships for both Q_{ON} and Q_{OFF} are fitted to single exponential functions (continuous lines). The calculated Q_{ON} time constants were 12.7 ms for pulses to −10 mV, and 2.3 ms for pulses to +20 mV.

Figure 3 further demonstrates charge movement conservation in WT FDB fibres. Charge movement currents were recorded in response to depolarizing pulses of different duration (starting at 2 ms and increasing in 2 ms increments) to −10 mV (Fig. 3*A* top), where we typically saw a pronounced temporally delayed component in WT fibres, and to +20 mV (Fig. 3*A* bottom), where a temporally delayed component was not apparent. Figure 3*B* shows the relationship between Q_{ON} or Q_{OFF} and pulse duration for the set of pulses in Fig. 3*A*. The normalized charge-pulse duration relationship was fitted to a single exponential function (continuous lines) of the form:

$$y = A_1 \times \exp(-x/t) + y_0 \qquad (1)$$

The calculated Q_{ON} time constants were 12.7 ms for pulses to −10 mV, and 2.3 ms for pulses to +20 mV. Similar values were obtained for Q_{OFF}.

Charge movement in S100A1 KO fibres lacks the temporally delayed, steeply voltage-dependent Q_γ component

Figure 4*A* shows the average charge *vs.* voltage (Q–V) relationship of 12 WT and 11 KO fibres. Consistent with simple visual comparison of charge movement currents between WT and KO fibres, the Q–V relationship was very similar between groups for steps to −70 to −30 mV. However, at −20 mV the data began to diverge and the charge moved in WT fibres (Q_{WT}) was considerably larger than their KO counterparts (Q_{KO}), consistent with the development of a second component. As a first approximation, the Q–V relationship of each individual fibre tested was fitted to a single Boltzmann function, as described by the equation:

$$Q(V) = Q_{max}/(1 + \exp((V_{half} - V)/k)), \qquad (2)$$

where Q_{max} gives the maximum charge movement, V_{half} defines the potential where $Q = 0.5$ of Q_{max} and $1/k$ is a measure of the steepness of the Q–V relationship. The KO data were typically well fitted by a single Boltzmann, with average Boltzmann parameters of $Q_{max} = 37.3 \pm 3.2$ nC μF^{-1}, $V_{half} = -25.8 \pm 1.04$ mV and $k = 13.0 \pm 0.9$ mV. A single Boltzmann fit to each WT data set gave average parameters of $Q_{max} = 53.0 \pm 4.9$ nC μF^{-1}, $V_{half} = -21.5 \pm 2.5$ mV and $k = 9.5 \pm 0.5$ mV. Using these parameters both Q_{max} and k values were found to be significantly different between WT and KO fibres ($P = 0.016$ and $P = 0.003$, respectively).

Upon inspection of the fits to the average data in Fig. 4*A*, it is clear that while a single Boltzmann function accurately fits the KO data ($R^2 = 0.998$), several points are missed along the WT curve ($R^2 = 0.955$). Based on the similar Q–V relationship of WT and KO fibres at lesser depolarizations and the presence of a second, Q_γ component of charge movement seen in WT, but not KO fibres, a double Boltzmann fit was applied to the WT data:

$$Q(V) = (Q_1/Q_{max})/(1 + \exp((V_{half,1} - V)/k_1)) + (Q_2/Q_{max})/(1 + \exp((V_{half,2} - V)/k_2))), \qquad (3)$$

where Q_{max} is the limiting charge movement, Q_1 and Q_2 are the amplitudes of the charge components, and V_{half} and k are half-activation voltage and slope factor for each component, respectively. For this fit we used all fixed Q_1, $V_{half,1}$, and k_1 parameters from the KO fibres for the first Boltzmann component and allowed free values for the

potential (HP) of −120 mV indicates negligible non-linearity of membrane properties over voltage range used to obtain leak templates with the *P*/4 leak subtraction protocol. *E*, non-linear capacitive current elicited by a test pulse of 80 mV amplitude (from −80 mV to 0 mV; top current trace) using *P*/4 method. Below is the amplitude of the *P*/4 leak template (Control, middle current trace) and full leak template (Control × 4; bottom current trace) for comparison.

second component. As can be seen in Fig. 4*B*, this double Boltzmann function very accurately fitted the WT data ($R^2 = 0.998$). As all parameters were fixed to KO values for the first component, the improved fit cannot be attributed to an increased number of free parameters; instead it appears the WT and KO data contained a very similar first component, with a second component only present in the WT fibres. The second component of the double Boltzmann fit displayed a steep voltage dependence, with parameters of $Q_{max} = 15.2$ nC μF^{-1}, $V_{half} = -13.0$ mV and $k = 4.8$ mV. A curve of this theoretically derived difference component ($Q_{WT\text{-}KO}$) is simulated in green, and represents Q_γ suppressed in the KO fibres.

To evaluate the properties of the current elicited by the difference component of charge movement we subtracted the average KO current records from the average WT current records for each depolarizing voltage step. This average difference current, $I_{WT\text{-}KO}$, is plotted *vs.* the average WT and KO charge movement currents (I_{WT} and I_{KO}, respectively) in Fig. 5. $I_{WT\text{-}KO}$ was negligible with steps to -70 through -40 mV. At -30, and more prominently -20 mV, $I_{WT\text{-}KO}$ began to develop a temporally delayed 'hump' which further increases in amplitude and area with steps to -10 and 0 mV while shifting back to earlier in time during the pulse. This current saturates in area around 0 mV.

To quantify $Q_{WT\text{-}KO}$ we subtracted the average I_{KO} record from individual I_{WT} records for steps to -50 through $+20$ mV. We then integrated the resulting difference records to get a Q–V relationship for each individual difference component. These Q–V relationships were averaged and fitted to a single Boltzmann function, as plotted in Fig. 6*A* (AVG Q–V fit). The curve displays parameters $Q_{max} = 12.1$ nC μF^{-1}, $V_{half} = -17.7$ mV and $k = 5.0$, which agree nicely with the steeply voltage-dependent component theoretically derived in Fig. 4*B*. The individual $Q_{WT\text{-}KO}$ Q–V relationships were also fitted to single Boltzmann functions, and their subsequent Boltzmann parameters averaged. These revealed average parameters of $Q_{max} = 12.9 \pm 2.4$ nC μF^{-1}, $V_{half} = -17.4 \pm 2.9$ mV and $k = 3.7 \pm 0.6$ mV. A simulated curve from these average parameters (AVG of Fits) is superimposed over the fit of the average Q–V relationship. The most noticeable difference in the curves was the increased steepness of the fit to the average parameters, quantified by the lower k value. The fit to the average Q–V relationship was slightly less steep due to the variable appearance of Q_γ along the voltage axis, which manifested itself as a larger range for V_{half} (range $= -27$ mV to -10 mV) and blurring of the steepness of the curve. This slight variability in the voltage dependence of Q_γ also accounted for the larger variation in WT V_{half} parameters compared to KO V_{half} parameters. Furthermore, it blurred the kinetic properties of the two distinct components in WT fibres when viewed as an average current record (Fig. 5). A more accurate visual depiction of the two temporal components is seen in traces from individual fibres, as in Fig. 1*A*, Fig. 7*B* and Fig. 9*B*. Figure 6*B* plots $Q_{WT\text{-}KO}$ *vs.* Q_{WT} and Q_{KO} for comparison. Figure 6*C* plots the Q–V curves normalized to Q_{max}, allowing a better visualization of the steeply voltage dependent difference component.

It is important to note that there was some variability in the presence or absence of the Q_γ component within the groups of KO and WT fibres. Two out of a total of 11 KO fibres *did* show clear indications of a delayed Q_γ

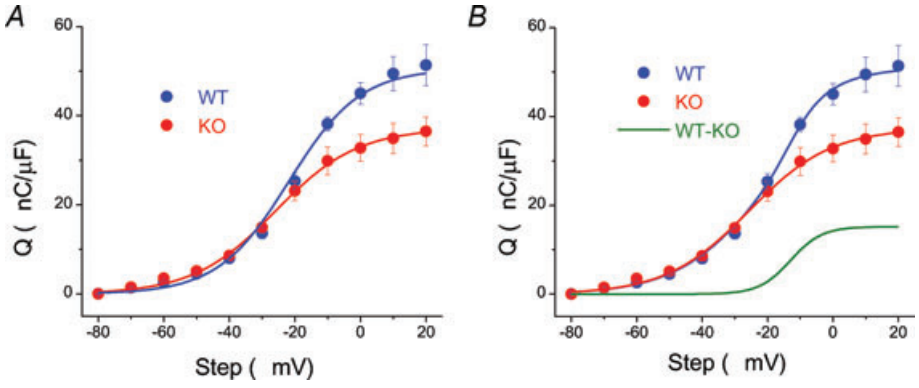

Figure 4. *Q–V* relationship of WT (blue) and KO (red) fibres
A, KO data was well fitted by a single Boltzmann function with parameters of $Q_{max} = 37.3$ nC μF^{-1}, $V_{half} = -25.8$ mV and $k = 12.6$; $n = 11$ fibres. A single Boltzmann function did not accurately fit the WT data. *B*, based on the second, temporally delayed component of charge movement seen in WT, but not KO fibres, a double Boltzmann fit was applied to the WT data using fixed KO parameters for the first Boltzmann function and free values for the second component. This double Boltzmann function very accurately fitted the WT data. The second component, analogous to the theoretically derived difference component, had Boltzmann parameters of $Q_{max} = 15.2$ nC μF^{-1}, $V_{half} = -13.0$ mV and $k = 4.8$; $n = 12$ fibres. A curve with these parameters is simulated in the WT – KO (green) trace.

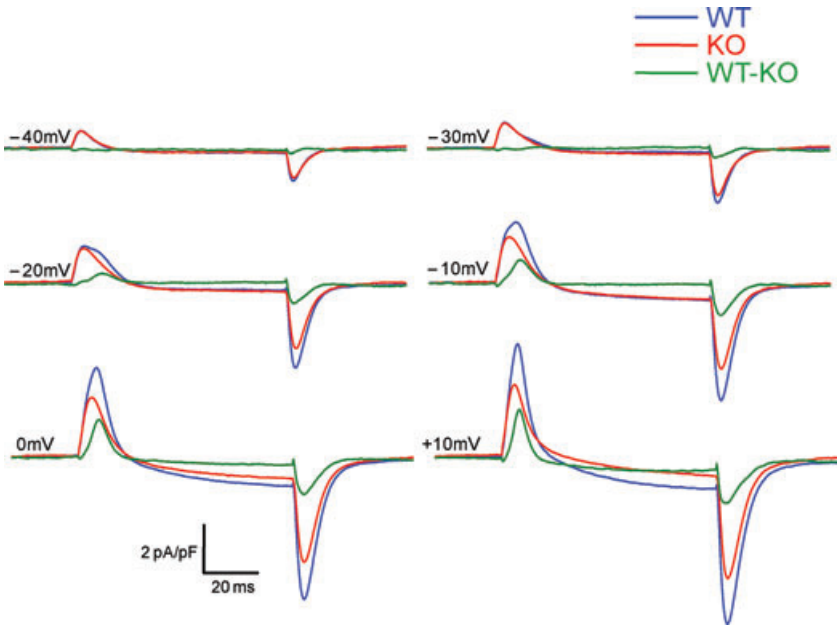

Figure 5. Average recordings of WT (blue) and KO (red) fibres plotted in time with average difference records (green)
Note virtually identical charge movement recordings at −40 and −30 mV steps, followed by development of delayed, steeply voltage dependent hump component (Q_γ) suppressed in KO fibres. At steeper depolarizations this component shifts back earlier in time and saturates in area.

component at one or more intermediate depolarization, and 1 out of 12 WT fibres *did not* exhibit a clear delayed Q_γ component over the same voltage range.

Thus, the presence or absence of the delayed Q_γ component is not absolutely determined by the presence of absence of S100A1. In the companion paper we show that the presence of the delayed Q_γ component in a few atypical KO fibres and its absence in a few atypical WT fibres is correlated with a relatively larger Ca^{2+} release in these atypical KO fibres, and a relatively smaller Ca^{2+} release in the atypical WT fibres. If these atypical fibres were excluded from the Boltzmann fits to the *Q vs. V* data sets for each individual fibre, the mean parameter values for the KO fibres (without noticeable delayed Q_γ component) were $Q_{max} = 34.2 \pm 2.6$ nC μF^{-1}, $V_{half} = -25.8 \pm 1.1$ mV and $k = 13.8 \pm 0.8$ mV. Excluding the atypical WT fibres lacking clear Q_γ and using mean Q_1 parameter values obtained only from KO fibres without any obvious delayed Q_γ component, the mean parameter values for the second charge component from the double Boltzmann fit are $Q_{max} = 16.1 \pm 2.6$ nC μF^{-1}, $V_{half} = -16.1 \pm 3.1$ mV and $k = 2.8 \pm 0.4$ mV.

These refined values are likely to reflect a better estimate of Q_β and Q_γ than obtained by using all KO fibres to define Q_β and all WT fibres (together with all KO fibres for Q_β) to define Q_γ.

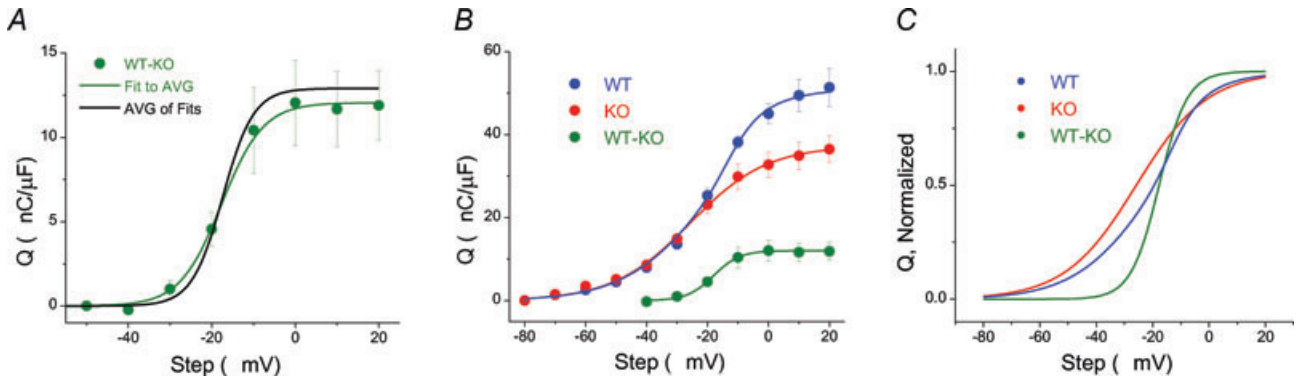

Figure 6 The *Q–V* relationship of WT–KO difference component, Q_γ
A, the average KO recording was subtracted from each individual WT current trace, and the resulting difference trace was integrated to establish *Q* during the step. The green trace represents the fit to the average difference *Q–V*, with Boltzmann parameters of $Q_{max} = 12.1$ nC μF^{-1}, $V_{half} = -17.7$ mV and $k = 5$, similar to those from the theoretically isolated difference component seen in Fig. 3*B*. The black trace is the slightly steeper curve generated from averaging the Boltzmann parameters of the individual fits to the difference *Q–V*s. *B*, average difference (WT – KO) *Q–V* plotted in scale with WT and KO *Q–V* relationships from Fig. 3*B*. *C*, normalized *Q–V* relationships of fits from panel *B*.

Intracellular application of S100A1 protein restores Q_γ in S100A1 KO fibres

Next we sought to evaluate whether the Q_γ component of charge movement suppressed in the KO fibres could be rescued by transient intracellular application of S100A1. To this end, we dialysed KO fibres with purified S100A1 protein and recorded charge movement currents. After our standard 20 min dialysis time, but now with 10 μM Alexa-488-S100A1 added to the pipette solution, non-linear capacitive currents were recorded using the same pulse protocol as detailed in the description of Fig. 1. Additionally, a confocal fluorescence image was taken of the dialysed fibre and a second image was taken of the tip of the pipette. Comparing the fluorescence in the pipette (with a known 10 μM Alexa-488-S100A1) to that of the fibre we could estimate the protein concentration achieved in the cell at the time of the recordings. The mean concentration of purified Alexa-488-S100A1 in the fibre at the time of charge movement recordings was 2.8 ± 0.2 μM, approximating the concentration of endogenous S100A1 in fast twitch skeletal muscle (Haimoto & Kato, 1987; Zimmer *et al.* 1991). As can be seen in Fig. 7*A*, dialysis of S100A1 into KO fibres almost completely restored the Q–V relationship of charge movement to the WT level, with restoration of both the total charge moved and the steepness of the curve. These data were well fitted by a double Boltzmann function ($R^2 = 0.998$), again using fixed KO parameters for the first Boltzmann and free parameters for the second. The restored (second) component obtained from this fit demonstrated Boltzmann parameters of $Q_{max} = 14.8$ nC μF^{-1}, $V_{half} = -12.7$ and $k = 6.1$, similar to the difference component between WT and KO fibres. Figure 7*B* compares the ON current record of a KO fibre dialysed with Alexa-488-S100A1 compared to the average KO fibre recording. It is clear that transient application of S100A1 can restore the kinetic properties of the charge movement current in KO fibres, as the characteristic temporally delayed hump component of charge movement becomes evident after application of S100A1.

S100A1$^{-/-}$ fibres do not have significant alteration in L-type channel expression or Ca^{2+} current activation

Suppressed maximal charge movement could be the result of decreased DHPR expression in KO muscle. To test this hypothesis, we performed Western blot analysis for the α_1s subunit of the DHPR in WT and KO muscle lysates. Figure 8*A* shows that protein expression of the DHPR was not altered in KO muscle, suggesting that decreased channel expression did not account for the differences in charge movement seen in KO fibres. Moreover, although S100A1 KO fibres lack Q_γ, they did not exhibit any noticeable difference in both the amplitude and the activation of L-type Ca^{2+} currents compared to WT fibres. Figure 8*B* presents representative time courses of Ca^{2+} currents from WT and KO fibres in response to 1 s depolarizing steps to −60 mV to +20 mV as illustrated above the graph. Current onset was slow and maximum inward current peaked at approximately 80 ms with a pulse to 0 mV. The voltage dependence of activation and peak current density appear similar between WT and KO fibres. The current *vs.* voltage (I–V) relationship for pooled data from 11 WT and eight KO fibres is shown in Fig. 8*C*. There were no significant differences in current density at any of the voltages tested, including the maximum inward current elicited by a step to 0 mV (WT $I_{Ca} = -5.8 \pm 0.5$ pA pF^{-1}, KO $I_{Ca} = -5.1 \pm 0.5$ pA pF^{-1}, $P = 0.27$). I–V plots from WT and KO fibres were fitted to a Boltzmann Ohmic function, described by the following equation (Nakai *et al.* 1996):

$$I = G_{max}(V - V_{rev})/[1 + \exp(-(V - V_{half})/k)], \quad (4)$$

where G_{max} is the maximum conductance, V is the membrane potential, V_{rev} is the reversal potential, V_{half}

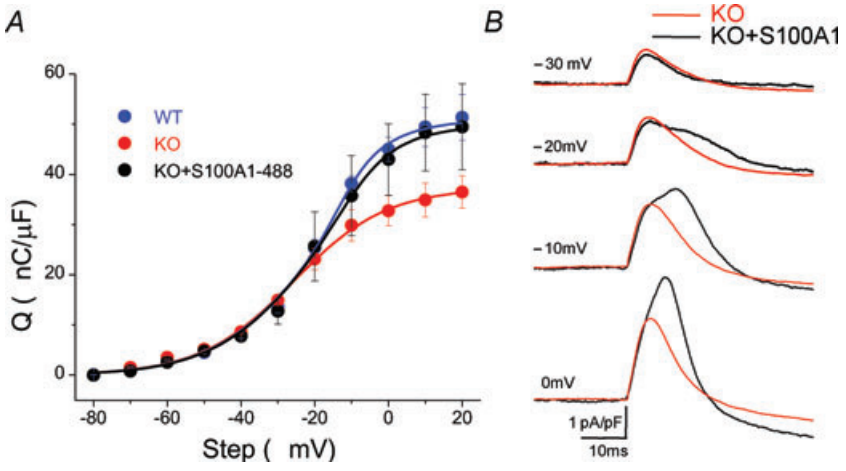

Figure 7. Rescue of Q_γ with purified S100A1
A, KO fibres dialysed, via the patch pipette, with 10 μM Alexa-488-S100A1 show restoration of Q–V relationship to WT levels. S100A1 protein concentration in KO fibres was estimated using confocal fluorescence microscopy and averaged 2.8 ± 0.21 μM at the time of recordings. *B*, zoom in of ON current traces from KO AVG and representative KO + S100A1 fibre show that kinetic properties of charge movement currents can be restored in KO fibres dialysed with S100A1, specifically the temporally delayed Q_γ component.

is the half-activation potential, and k is a measure of the steepness. Average parameter values for G_{max}, V_{half} and k for WT fibres were 108.7 pS pF^{-1}, −14.7 mV and 5.4 mV, respectively. For KO fibres G_{max}, V_{half} and k were 106.0 pS pF^{-1}, −9.6 mV and 7.6 mV, respectively. These parameters were used to derive the activation curves for WT and KO fibres, as plotted in Fig. 8*C* (bottom). Other than a slight rightward shift in the V_{half} of KO fibres, there were no noticeable differences in L-type current activation. This suggests that despite suppression of Q_γ in KO fibres, the activation of L-type Ca^{2+} currents was not significantly affected.

Application of dantrolene suppresses the Q_γ component in WT fibres

It has been suggested that the Q_γ component of charge movement identified in amphibian fibres is a consequence of Ca^{2+} released from the SR (Csernoch *et al.* 1991). If the decreased charge movement in KO fibres is a consequence of their decreased Ca^{2+} release (Most *et al.* 2003; Prosser *et al.* 2007), then a pharmacological intervention that reduces Ca^{2+} release should suppress the second component of charge movement. Therefore, we sought to reduce Ca^{2+} release with dantrolene, an inhibitor of RyR1, and measure the effect on charge movement. To this end we first identified a suitable concentration of dantrolene that mimicked the reduction of the Ca^{2+} transient inherent to fibres lacking S100A1. As shown in Fig. 9*A*, we found that after 3 min exposure to 40 μM dantrolene the peak amplitude of the action potential evoked Ca^{2+} transient was reduced by about 35%. The effect was consistent, relatively stable over time, and in general mimicked the reduction of the Ca^{2+} transient previously reported for fibres lacking S100A1 (Prosser *et al.* 2007). We then recorded the effect of

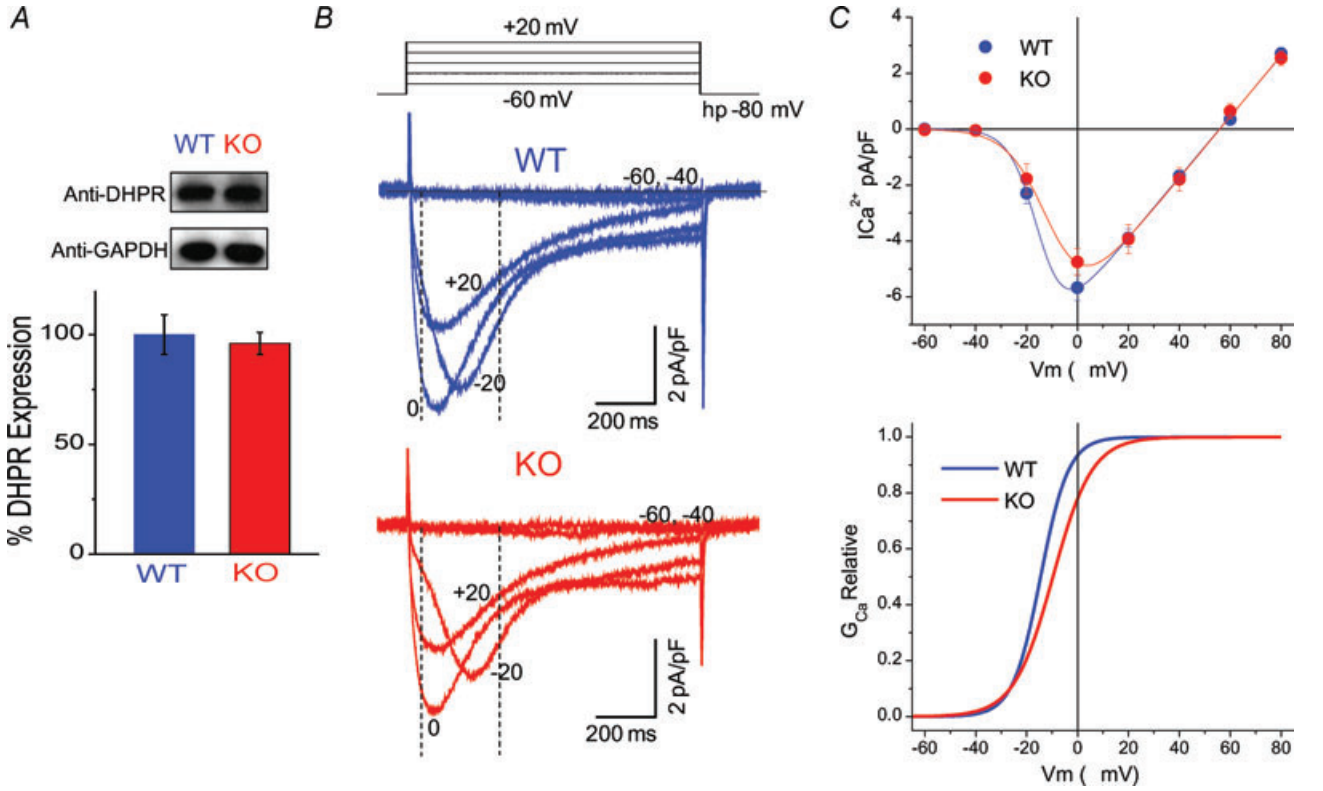

Figure 8. L-type Ca^{2+} current density, voltage dependence and channel expression are not significantly changed in KO fibres

A, representative Western blots with anti-α_1s from lysates of WT and S100A1$^{-/-}$ muscle show similar DHPR expression, with GAPDH used as a loading control. The bar graph is the result of triplicate experiments in WT and KO muscle, showing that the expression of the DHPR is not altered with the ablation of S100A1. Data are presented as a percentage of the average WT DHPR expression, normalized to the GAPDH signal. *B*, representative macroscopic Ca^{2+} current recordings of WT (blue) and KO (red) fibres. In these experiments Cd^{2+} and Co^{2+} were eliminated from the external solution and Ca^{2+} was increased to 2 mM. Vertical dashed lines illustrate the time used to measure peak current values to create the *I–V* plots. *C*, top, *I–V* relationship of average data from WT and KO fibres reveals no significant differences in L-type channel current density and voltage dependence. The data are fitted to a Boltzmann-Ohm function. At bottom is the activation profile of WT and KO fibres derived from parameters of a Boltzmann-Ohm function. These results suggest that suppressed charge movement in KO fibres is not linked to changes in L-type Ca^{2+} channel expression and voltage-dependent activation.

this concentration of dantrolene on charge movement in control fibres. Figure 9*B* (left) shows representative ON charge movement currents of a control fibre before and after 3 min exposure to dantrolene, and the resulting difference record. Exposure to dantrolene did not affect the first component of charge movement but at least partially suppressed the temporally delayed component seen at intermediate depolarizations. Figure 9*B* (right) shows the average ON charge movement currents of four KO fibres before and after dantrolene, and the resulting difference current. There was no temporally delayed component in these KO fibres prior to exposure to dantrolene, and, notably, exposure to dantrolene caused no further suppression in charge movement in any of these fibres. The only detectable difference was a slight increase of the Q_β component of charge movement, as indicated by the minor negative deflection in the difference current. Figure 9*C* shows the pooled *Q versus V* relationship from six control fibres before and after treatment with dantrolene. The *Q–V* relationship of the integrated difference records is also displayed for comparison. The difference component over the voltage range of −50 mV to −10 mV was fitted by a single Boltzmann function with parameters $Q_{max} = 6.3$ nC μF^{-1}, $V_{half} = -21.5$ mV and $k = 3.0$ mV. It should be noted that this fit only accurately described the *Q vs. V* relationship of the

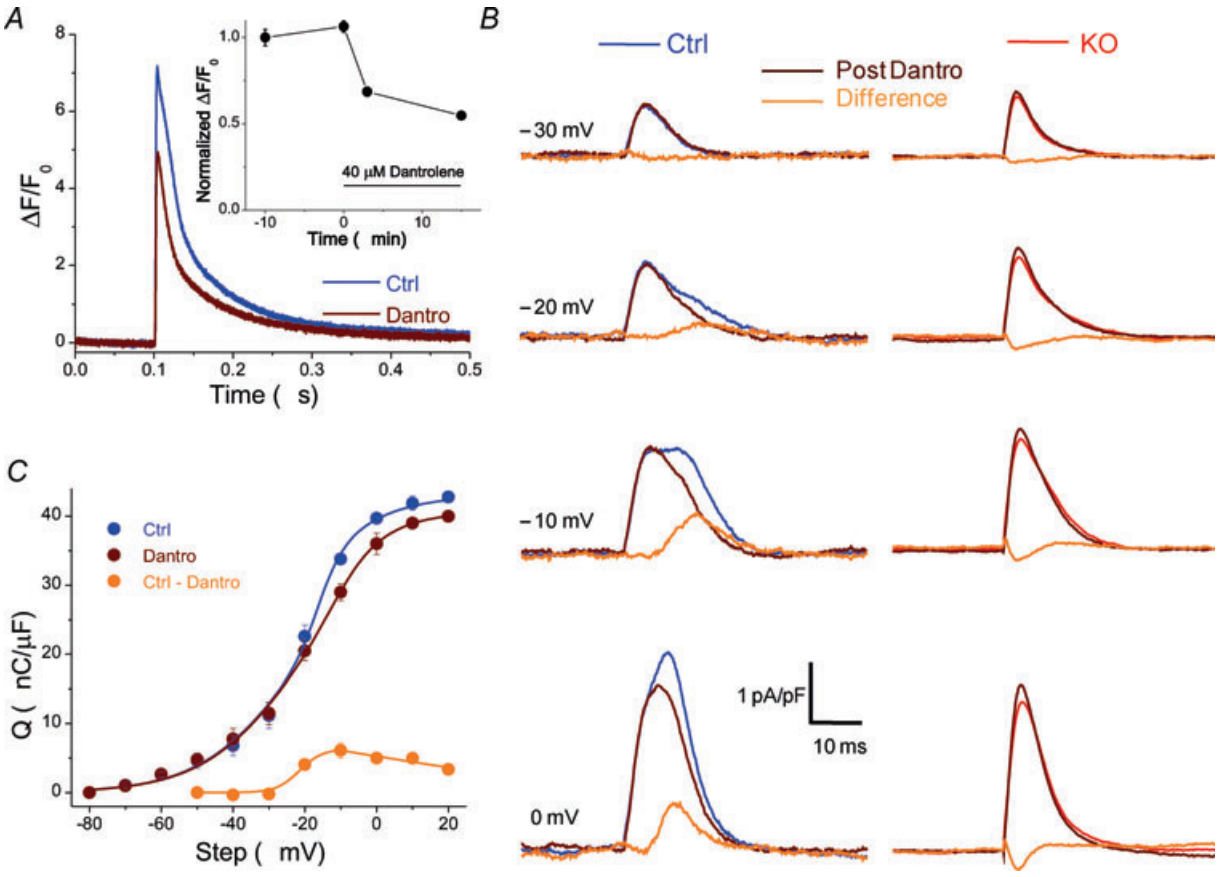

Figure 9. Effect of the RyR1 inhibitor dantrolene on charge movement
A, exposure of control fibres to 40 μM dantrolene for 3 min suppressed the action potential evoked Ca^{2+} transient by about 35%, measured with high speed confocal microscopy and Fluo4-AM Ca^{2+} indicator dye. This reduction in the Ca^{2+} transient recapitulates the suppression seen in KO fibres (Prosser *et al.* 2007). The inset shows the normalized peak values of the Ca^{2+} transient (reported as $\Delta F/F_0 \pm$ S.E.M.) as a function of time of exposure to dantrolene. *B*, charge movement currents from a control fibre (left), before (blue trace) and after (brown trace) 3 min exposure to 40 μM dantrolene in the bath, and the resulting difference current (orange trace). As can be seen, the RyR inhibitor dantrolene suppressed a temporally delayed hump component at intermediate voltages, without affecting the initial component of charge movement currents, similar to the difference current between WT and KO fibres. On the right of the figure are charge movement currents elicited by the same voltage steps in 4 KO fibres exposed to the same concentration of dantrolene (red traces). There was no suppression of charge movement in any of these fibres. *C*, *Q–V* relationship of 6 control fibres before and after treatment with dantrolene. The steeply voltage-dependent difference component (Ctrl – Dantro; orange *Q–V*) was fitted to a single Boltzmann function to −10 mV and displayed parameters $Q_{max} = 6.3$ nC μF^{-1}, $V_{half} = -21.5$ mV and $k = 3.0$ mV. At higher voltages the difference component decreased monotonically with voltage and was therefore fitted to a linear function.

dantrolene isolated difference component for steps to −50 mV to −10 mV. Upon further depolarizations the difference component appears to decrease monotonically with voltage, and therefore has been fitted with a straight linear function over this voltage range. These findings suggest that 40 μM dantrolene partially suppresses and/or shifts the voltage dependence of Q_γ in control fibres to higher potentials, but has minimal or no affect on KO fibres which initially lack Q_γ.

La^{3+} profoundly modifies charge movement currents in FDB fibres, but Cd^{2+} and Co^{2+} do not

As the temporally delayed Q_γ component of charge movement has not been consistently demonstrated in mammalian fibres, we next evaluated possible explanations for this discrepancy. Since Cd^{2+} has been suggested previously to alter the kinetic properties of charge movement (Francini *et al.* 2001), we first evaluated charge movement in the absence of Cd^{2+} and Co^{2+} by using our standard internal and external solutions, except with the elimination of Cd^{2+} and Co^{2+} from the external solution. To block inward Ca^{2+} currents and allow the evaluation of charge movement currents, we added 10 mM Mg^{2+} to the external solution. This set of control experiments, both for Cd^{2+}/Co^{2+} and for La^{3+} (see below), were carried out on FDB fibres from mice of the C57Black strain. Figure 10*A* shows representative recordings from one such control fibre bathed in the high Mg^{2+}, Cd^{2+} and Co^{2+} free external solution. The presence of a temporally delayed 'hump' component is clearly evident in the current records at similar voltages to where it is typically seen in control fibres bathed in our standard Cd^{2+}/Co^{2+} based external solution. Figure 10*B* shows the pooled *Q vs. V* relationship of three control fibres exposed to high Mg^{2+}, Cd^{2+} and Co^{2+} free external solution and three control fibres exposed to Cd^{2+}/Co^{2+}solution. The *Q vs. V* relationship of fibres treated with high Mg^{2+}, Cd^{2+} and Co^{2+} free solution was very similar in both slope and amplitude to that of fibres exposed to Cd^{2+}/Co^{2+}, with only a slight, 2–3 mV shift in the half-maximal voltage. The data were fitted by a double Boltzmann function with the following parameters: $Q_{max,1} = 33.8$ nC μF^{-1}, $Q_{max,2} = 14.2$ nC μF^{-1}, $V_{half,1} = -19.0$ mV, $V_{half,2} = -13.0$ mV, $k_1 = 12.8$ mV and $k_2 = 4.0$ mV.

La^{3+} is another common and widely used Ca^{2+} channel blocker. In preliminary experiments using a recording solution containing La^{3+} we did not detect the presence of two kinetically distinct components of charge movement in FDB fibres. We therefore sought to further evaluate the effects of La^{3+} on charge movement. Figure 10*C* shows representative charge movement currents from fibres exposed to 0.3 mM La^{3+} in our standard external solution containing Cd^{2+}/Co^{2+}. These fibres exhibited dramatically increased current kinetics and did not display any clear temporally delayed 'hump' component in the current records. Figure 10*D* plots the *Q vs. V* relationship of pooled data from five control fibres exposed to La^{3+} compared with the control fibres exposed to Cd^{2+}/Co^{2+} from Fig. 10*B*. As a first approximation the La^{3+} *Q vs. V* data were fitted to a single Boltzmann function, with parameters $Q_{max} = 27.0$ nC μF^{-1}, $V_{half} = -10.4$ mV and $k = 16.6$ mV, $R^2 = 0.987$. Therefore, the addition of La^{3+} led to a reduction in both Q_{max} and the steepness of the *Q vs. V* relationship, as well as a rightward shift in the voltage dependence of charge movement.

Figure 10*E* compares charge development with increasing pulse duration from a step to −10 mV in a fibre treated with our standard external solution (top) *vs.* one supplemented with 0.3 mM La^{3+} (bottom). A temporally delayed hump component is clearly distinguishable in the fibre exposed to Cd^{2+}/Co^{2+}, and noticeably absent in the La^{3+} exposed fibre, which exhibits markedly increased current kinetics. Figure 10*F* plots the charge *vs.* pulse duration relationship for these two fibres. The calculated time constant for charge development in the Cd^{2+}/Co^{2+} exposed fibre was 13 ms, compared to 2.4 ms for the fibre exposed to La^{3+}. Thus the addition of La^{3+} to our standard external solution dramatically increased the kinetics of charge movement and decreased the amount of charge moved in control fibres.

Discussion

Gating charge movement in muscle

Gating charge movement was first predicted by Hodgkin & Huxley (1952) to explain the voltage-dependent origin of Na^+ and K^+ conductance in the nerve. The first recordings of these gating currents were applied to the activation of muscle contraction by Schneider & Chandler (1973), who proposed that voltage-dependent intra-membrane charge movement was a key step in skeletal muscle EC coupling. Evidence has accumulated demonstrating that the α1 subunit (α_{1S}) of the DHPR is the primary source of this charge movement (Tanabe *et al.* 1988; Nakai *et al.* 1996) that triggers Ca^{2+} release from the mechanically linked RyR1 (Block *et al.* 1988; Protasi *et al.* 2002) and promotes skeletal-specific muscle contraction (Horowicz & Schneider, 1981*a*).

While the majority of the seminal work on muscle charge movement was done in amphibian fibres, recently the focus has switched to mammalian muscle and expression systems. One striking difference between recordings in amphibian and mammalian muscle is the kinetic properties of charge movement currents. In amphibian fibres two distinct components of charge movement have repeatedly been identified: a relatively fast initial component, Q_β, and a temporally delayed 'hump'

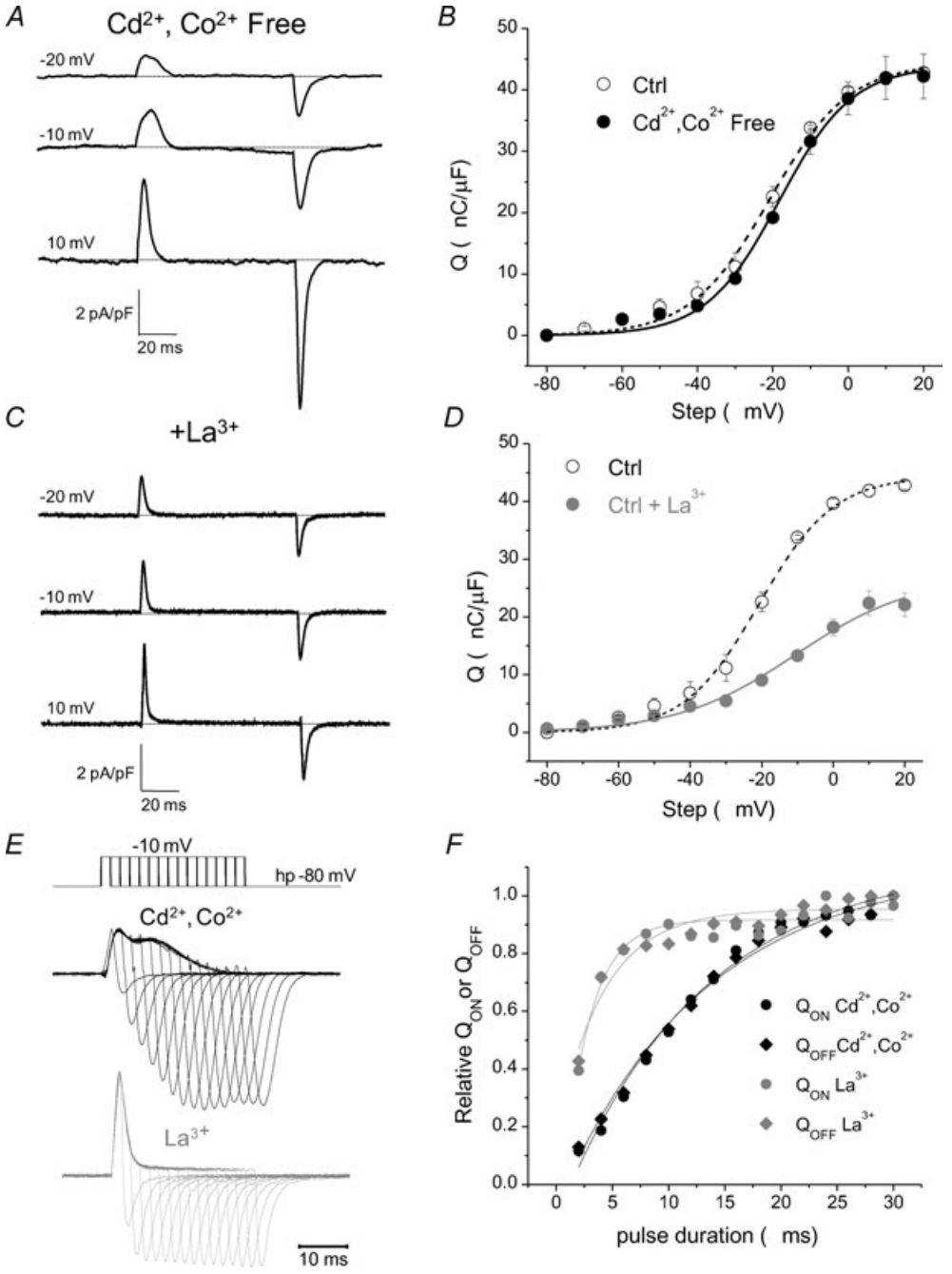

Figure 10. La^{3+} profoundly modifies intra-membrane charge movement
A, charge movement currents recorded using an external solution lacking Cd^{2+} and Co^{2+} exhibit a temporally delayed component and similar current kinetics to fibres bathed in our standard control solution. Ca^{2+} was reduced to 0.5 mM and 10 mM Mg^{2+} was added to the external solution to block inward ionic components. *B*, fibres bathed in control external solution (open circles, dashed line) demonstrate a very similar *Q vs. V* relationship to fibres bathed in Cd^{2+} and Co^{2+} free external solution (filled circles, continuous line). *C*, charge movement currents recorded using an external solution supplemented with 0.3 mM La^{3+} exhibit rapid current kinetics and no clear temporally delayed 'hump' component. *D*, fibres bathed in our control external solution supplemented with La^{3+} demonstrate decreased maximal charge moved and a rightward shift in the voltage dependence of charge movement when compared to fibres bathed in our standard external solution. *E*, charge movement currents recorded in control and La^{3+}-treated fibres in response to depolarizing pulses to −10 mV of increasing duration (2 ms increments) to evaluate charge movement conservation. *F*, Q_{ON} or Q_{OFF} *vs.* pulse duration for the complete set of pulses of corresponding traces illustrated in *E*. The normalized charge–pulse duration relationships for both Q_{ON} and Q_{OFF} are fitted to single exponential functions (continuous lines). The calculated time constant for charge development in the Cd^{2+}/Co^{2+} exposed fibre was 13 ms, compared to 2.4 ms for the fibre exposed to La^{3+}.

component, Q_γ (Adrian & Almers, 1976; Horowicz & Schneider, 1981*a*; Melzer *et al.* 1986; Csernoch *et al.* 1991; Jong *et al.* 1995). On the contrary, in charge movement recordings in mammalian fibres and myotubes Q_γ has been conspicuously absent; charge movement currents appear generally as a rise to peak followed by a simple decay (Hollingworth & Marshall, 1981; Simon & Beam, 1985; Delbono *et al.* 1991; Wang *et al.* 1999; Avila & Dirksen, 2000; Bannister & Beam, 2005; Royer *et al.* 2008). It should be noted that Simon & Beam (1985) and Lamb (1986*a*) did report that in a minority of their mammalian fibres charge movement recordings exhibited a slight temporally delayed component resembling Q_γ, and Francini *et al.* (2001) were able to detect a delayed component in rat EDL muscle. However the overall discrepancy between amphibian and mammalian charge movement records remains unresolved.

Recent groups using the whole cell patch-clamp technique on FDB fibres have demonstrated charge movement currents with a single rise and simple decay (Wang *et al.* 1999, 2002; Royer *et al.* 2008). Here using this same technique we demonstrate a clear, consistent, temporally delayed component in the ON charge movement currents of WT murine FDB fibres. As an explanation for this discrepancy, we propose that the use of the trivalent cation lanthanum as a Ca^{2+} channel blocker (Wang *et al.* 1999, 2002; Royer *et al.* 2008) may alter charge movement currents and mask Q_γ in mammalian fibres. We use a channel blocking cocktail of Cd^{2+} and Co^{2+}, with no added La^{3+}, to minimize ionic currents; in our hands the addition of La^{3+} dramatically increased the kinetics of charge movement currents and abolished any temporally distinct components (Fig. 10*C*, *E* and *F*), leaving recordings that kinetically resemble those of these recent reports. We also noted a reduction in the maximum charge moved (Q_{max}) and rightward shift in the voltage dependence of charge movement (V_{half}) in the presence of La^{3+}, when compared to our control solution. The La^{3+} Q_{max} value reported here is about 30% less than that reported by Wang *et al.* (1999) and Royer *et al.* (2008). Potential explanations for this discrepancy include different strains and age (5–7 weeks here *vs.* 5–7 months in the study of Wang *et al.*) of mice studied. Additionally, the studies by both Wang *et al.* and Royer *et al.* used a higher concentration of Mg^{2+} in their external solution (2 and 3.5 mM, respectively) than our 1 mM Mg^{2+}. Increased Mg^{2+} could potentially blunt some of the effects of La^{3+} on the voltage sensor. A final possibility to consider is that part of the decrease in charge movement seen here in the La^{3+} containing solution could be due to a partial detubulation of the fibres in La^{3+}. There was a slight, but not significant, decrease in the total fibre linear capacitance from 1.33 ± 0.05 nF and 1.32 ± 0.05 nF for WT and KO fibres ($n = 38$ and 29, respectively) measured in our standard external solution to 1.20 ± 0.11 nF for the 13 fibres measured in La^{3+} containing solution ($P = 0.24$), indicating that detubulation was likely not to be a major factor. To our knowledge the effects of La^{3+} on skeletal EC coupling have not been thoroughly explored; however La^{3+} has been shown to alter both sodium and potassium voltage-dependent channel gating in a manner that cannot be explained by surface charge considerations alone (Armstrong & Cota, 1990; Tytgat & Daenens, 1997). We additionally observed both time- and use-dependent effects of La^{3+} on charge movement currents and therefore suggest that the use of this trivalent cation as an L-type Ca^{2+} channel blocker should be approached with caution.

Effects of S100A1 on voltage sensor charge movement

A striking finding of this work is the modulation of intra-membrane charge movement by an endogenous Ca^{2+} binding protein, S100A1. Q_γ was selectively suppressed in fibres lacking S100A1, resulting in reduced sensitivity to activation (decreased steepness of the Q–V relationship), and reduced maximal activation (decreased Q_{max}) of the voltage sensor. Notably, the first component of charge movement (Q_β) appeared unaffected by ablation of S100A1, as can be seen by the identical current traces at voltages hyperpolarized to the development of Q_γ (Fig. 4), as well as by the accurate double Boltzmann fit to the WT Q–V relationship with fixed KO parameters describing the first component. These data suggest a selective suppression of a distinct component of charge movement in fibres lacking S100A1.

Moreover, several lines of evidence presented here support that effects on charge movement appear to be specific to S100A1, and not a result of compensatory changes in KO animals. First, a 20 min intracellular application of S100A1 restored both the total charge moved and the kinetics of Q_γ in KO fibres, arguing against a developmental role of S100A1 in the modulation of charge movement. Second, Western blot analysis suggests that protein expression of the DHPR is not changed in KO fibres. Third, the L-type Ca^{2+} current density and voltage-dependent activation do not appear to be significantly altered in KO fibres. The last two pieces of evidence suggest that the total expression of DHPR Ca^{2+} channels, as well as the functional fraction of these Ca^{2+} channels, is preserved in fibres lacking S100A1, implying that the suppressed charge in KO fibres is independent of channel expression and/or developmental or compensatory changes due to genetic manipulation. This is a unique finding, as multiple groups have demonstrated a reduction in charge movement with the alteration of endogenous proteins, but as a by-product of reduced functional L-type channels. For

example, mutations to the $\beta 1$ subunit of the DHPR lead to reduced α_{1S} expression at the membrane and a concomitant decrease in charge movement (Gregg *et al.* 1996; Schredelseker *et al.* 2009), and expression of the RGK family member Rem reduces the functional number of DHPRs and charge movement in myotubes (Bannister *et al.* 2008). To our knowledge, this specific modulation of gating charge by S100A1 is the first example of an endogenous protein regulating skeletal muscle charge movement independent of channel expression.

This reduction in charge movement is consistent with our previous findings that fibres lacking S100A1 have depressed SR Ca^{2+} release (Prosser *et al.* 2007). In that work we showed that action potential evoked Ca^{2+} transients are smaller in KO fibres compared to WT counterparts, a finding predicted if there is decreased activation of the voltage sensor. Additionally, as DHPR expression levels and L-type Ca^{2+} currents in KO fibres do not differ from their WT counterparts (Fig. 8*B* and *C*), the suppressed Q_γ component does not appear to be linked to gating of the DHPR Ca^{2+} channel, but instead is likely to be linked to the excitation–contraction coupling machinery. One interpretation of these findings is that S100A1 modulates intra-membrane voltage sensors that regulate Ca^{2+} release, but not the gating of the DHPR Ca^{2+} channel. However, we have also previously proposed that S100A1's modulation of Ca^{2+} release is a direct effect of S100A1 binding to RyR1 and enhancing RyR1 release. This was supported by previous reports of S100A1 increasing the open probability of the purified RyR1 in single channel recordings (Treves *et al.* 1997), and our demonstration, in conjunction with our collaborators, that S100A1 competes with calmodulin for binding the CaM binding domain (CaMBD) of RyR1 (Prosser *et al.* 2007; Wright *et al.* 2008), a site previously demonstrated to modulate the channel's activation (Tripathy *et al.* 1995; Moore *et al.* 1999; Rodney & Schneider, 2003).

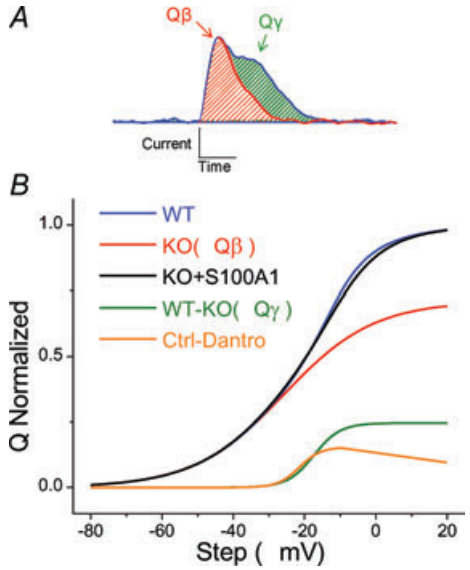

Figure 11. Components of charge movement in mammalian fibres
A, charge movement in WT fibres consisted of two components, the first eliciting a current with an initial rise to peak and simple decay, similar to Q_β (red), and the second, a temporally delayed, steeply voltage dependent component, similar to Q_γ (green). Q_γ was suppressed in fibres lacking S100A1, consistent with decreased RyR-mediated Ca^{2+} release. *B*, comparison of the *Q–V* relationships of WT (blue; total charge movement) and KO (red; Q_β) fibres, along with difference *Q–V* plot (WT−KO, green; Q_γ). Transient application of S100A1 restored Q_γ, suggesting that this suppression of charge movement is not due to developmental or compensatory effects of S100A1 KO (KO+S100A1, black). Inhibition of RyR with dantrolene also suppressed a temporally delayed, steeply voltage dependent component similar to Q_γ (Ctrl – Dantro, orange), suggesting this component may be a product of crosstalk between the voltage sensor of EC coupling, DHPR, and the mechanically coupled SR Ca^{2+} release channel, RyR. All curves are Boltzmann fits to average data.

While these two proposed mechanisms for S100A1's modulation of EC coupling may appear contradictory, they are not mutually exclusive. The DHPR and RyR interact in both an 'orthograde' manner, where the DHPR signals RyR1 to open, and a 'retrograde' fashion, where RyR1 prevents DHPR inactivation (Nakai *et al.* 1996). Interestingly, the CaMBD where S100A1 binds RyR1 is involved with mechanical coupling and bi-directional signalling with the DHPR. Specifically, the CaMBD of RyR1 interacts with the carboxyl-terminal tail of the DHPR (Sencer *et al.* 2001), and the region of RyR1 containing the CaMBD elicits a retrograde signal to the DHPR (Nakai *et al.* 1998). It is tempting to speculate that S100A1 interacting with this same region of RyR1 may affect retrograde coupling between the two proteins, enhancing voltage sensor activation and/or Ca^{2+} release. However, studies on retrograde signalling in myotubes suggest that while L-type Ca^{2+} currents are dramatically affected by interaction with RyR1, voltage sensor charge movement is minimally influenced, undermining this hypothesis (Nakai *et al.* 1996). Nonetheless, myotubes lack Q_γ and demonstrate less than 20% of the total charge moved in adult fibres (Nakai *et al.* 1998; Avila & Dirksen, 2000), validating the exploration of the interaction between the CaMBD of RyR1 and the DHPR and its effects on charge movement in adult fibres.

Origin of Q_γ

An alternative explanation for the enhanced charge movement in the presence of S100A1 is that Q_γ appears as a consequence of RyR-mediated Ca^{2+} release. This is not a novel concept; the nature of the delayed component has been widely debated. Several groups proposed Q_γ to be the primary charge moved by the voltage sensor that causes Ca^{2+} release (reviewed in Huang, 1988). Yet Q_γ has also been well argued to be a consequence of release, in a model put forth primarily by Pizarro *et al.* (1991). Our

findings with the RyR1 inhibitor dantrolene support this hypothesis. Dantrolene rapidly suppressed the temporally delayed hump in charge movement currents of control fibres, isolating a component with similar initial voltage dependence to the component suppressed in KO fibres. These results suggest that Q_γ may be a function of optimal RyR-mediated Ca^{2+} release. In KO fibres, where Q_γ is already suppressed (in conjunction with suppressed release, as is documented in the companion paper), dantrolene treatment caused no further suppression of charge, as would be expected if Q_γ is a consequence of optimal release.

However, our data with dantrolene treatment of control fibres do not completely mimic the difference in charge movement between WT and KO fibres. The difference component isolated by dantrolene peaks around −10 mV and then begins to decrease monotonically with voltage, suggesting a rightward shift in the voltage dependence of Q_γ. We cannot determine whether this difference component would diminish to zero upon further depolarization beyond +20 mV, mostly due to the presence of ionic contamination at these large depolarizations which precluded an accurate isolation of charge movement currents. In contrast to the dantrolene isolated component, we did not see rescue of Q_γ at larger depolarizations in KO fibres, where differences in maximal saturating charge in WT compared to KO fibres were maintained even at steps to +30 or +40 mV. These findings suggest a more complex mechanism than simply the amount of Ca^{2+} release dictating the presence or absence of Q_γ (with Q_γ defined here as the difference component between WT and KO fibres). A detailed examination of the relationship between charge movement and Ca^{2+} release in WT and KO fibres is needed to address these questions, and is provided in the companion paper (Prosser *et al.* 2009).

Regardless of this discrepancy, it is clear from our studies and previous work that Q_γ is selectively affected when the RyR1 Ca^{2+} release channel is altered (Lamb, 1986*b*; Hollingworth *et al.* 1990; Csernoch *et al.* 1991; García *et al.* 1991; Gonzalez & Rios, 1993). This does not appear to be a function of global myoplasmic $[Ca^{2+}]$, as all of our recordings were performed in high intracellular EGTA. Instead our data suggest a process, dependent on optimal RyR1 activation and/or local Ca^{2+} release, that can be modulated by S100A1, and that positively feeds back on voltage sensor charge movement. The mechanistic underpinnings of the relationship between S100A1, Ca^{2+} release and Q_γ are further explored in the companion paper.

Summary

In conclusion, here we demonstrate that mammalian muscle fibres exhibit two distinct components of intra-membrane charge movement (Fig. 11*A*), a relatively rapid initial rise to peak (Q_β), and a temporally delayed hump component (Q_γ). The use of La^{3+} as a Ca^{2+} channel blocker altered the kinetics and voltage dependence of intra-membrane charge movement. We showed that Q_γ is selectively suppressed in muscle fibres lacking S100A1 (Fig. 11*B*, red curve), a protein known to bind to RyR1 and enhance Ca^{2+} release. We also found that the RyR-inhibitor dantrolene selectively suppresses a similar component of voltage sensor charge movement (Fig. 11*B*, orange curve), suggesting that Q_γ may be a product of cross talk between RyR1 and DHPR. Transient application of S100A1 rescues Q_γ in KO fibres (Fig. 11*B*, black curve), suggesting a specific effect of S100A1 on charge movement. These results further support S100A1 as a positive regulator of the t-tubule voltage sensor and SR Ca^{2+} release channel in skeletal muscle-type EC coupling.

References

Ackermann GE, Domenighetti AA, Deten A, Bonath I, Marenholz I, Pedrazzini T, Erne P & Heizmann CW (2008). S100A1 deficiency results in prolonged ventricular repolarization in response to sympathetic activation. *Gen Physiol Biophys* **27**, 127–142.

Adrian RH & Almers W (1976). Charge movement in the membrane of striated muscle. *J Physiol* **254**, 339–360.

Adrian RH & Peres AR (1977). A gating signal for the potassium channel? *Nature* **267**, 800–804.

Armstrong CM & Cota G (1990). Modification of sodium channel gating by lanthanum. Some effects that cannot be explained by surface charge theory. *J Gen Physiol* **96**, 1129–1140.

Avila G & Dirksen RT (2000). Functional impact of the ryanodine receptor on the skeletal muscle L-type Ca^{2+} channel. *J Gen Physiol* **115**, 467–480.

Bannister RA & Beam KG (2005). The α1S N-terminus is not essential for bi-directional coupling with RyR1. *Biochem Biophys Res Commun* **336**, 134–141.

Bannister RA, Colecraft HM & Beam KG (2008). Rem inhibits skeletal muscle EC coupling by reducing the number of functional L-type Ca^{2+} channels. *Biophys J* **94**, 2631–2638.

Block BA, Imagawa T, Campbell KP & Franzini-Armstrong C (1988). Structural evidence for direct interaction between the molecular components of the transverse tubule/sarcoplasmic reticulum junction in skeletal muscle. *J Cell Biol* **107**, 2587–2600.

Chandler WK, Rakowski RF & Schneider MF (1976). A non-linear voltage dependent charge movement in frog skeletal muscle. *J Physiol* **254**, 245–283.

Csernoch L, Pizarro G, Uribe I, Rodríguez M & Ríos E (1991). Interfering with calcium release suppresses I_γ, the 'hump' component of intramembranous charge movement in skeletal muscle. *J Gen Physiol* **97**, 845–884.

Delbono O, García J, Appel SH & Stefani E (1991). Calcium current and charge movement of mammalian muscle: action of amyotrophic lateral sclerosis immunoglobulins. *J Physiol* **444**, 723–742.

Desjardins JF, Pourdjabbar A, Quan A, Leong-Poi H, Teichert-Kuliszewska K, Verma S & Parker TG (2009). Lack of S100A1 in mice confers a gender-dependent hypertensive phenotype and increased mortality following myocardial infarction. *Am J Physiol Heart Circ Physiol* **296**, H1457–1465.

Francini F, Bencini C, Piperio C & Squecco R (2001). Separation of charge movement components in mammalian skeletal muscle fibres. *J Physiol* **537**, 45–56.

García J, Pizarro G, Ríos E & Stefani E (1991). Effect of the calcium buffer EGTA on the 'hump' component of charge movement in skeletal muscle. *J Gen Physiol* **97**, 885–896.

Gonzalez A & Rios E (1993). Perchlorate enhances transmission in skeletal muscle excitation-contraction coupling. *J Gen Physiol* **102**, 373–421.

Gregg RG, Messing A, Strube C, Beurg M, Moss R, Behan M, Sukhareva M, Haynes S, Powell JA, Coronado R & Powers PA (1996). Absence of the β subunit (cchb1) of the skeletal muscle dihydropyridine receptor alters expression of the α1 subunit and eliminates excitation-contraction coupling. *Proc Natl Acad Sci U S A* **93**, 13961–13966.

Haimoto H & Kato K (1987). S100a0 (alpha alpha) protein, a calcium-binding protein, is localized in the slow-twitch muscle fibre. *J Neurochem* **48**, 917–923.

Hamill OP, Marty A, Neher E, Sakmann B & Sigworth FJ (1981). Improved patch-clamp techniques for high-resolution current recording from cells and cell-free membrane patches. *Pflugers Arch* **391**, 85–100.

Hodgkin AL & Huxley AF (1952). A quantitative description of membrane current and its application to conduction and excitation in nerve. *J Physiol* **117**, 500–544.

Hollingworth S & Marshall MW (1981). A comparative study of charge movement in rat and frog skeletal muscle fibres. *J Physiol* **321**, 583–602.

Hollingworth S, Marshall MW & Robson E (1990). The effects of tetracaine on charge movement in fast twitch rat skeletal muscle fibres. *J Physiol* **421**, 633–644.

Horowicz P & Schneider MF (1981*a*). Membrane charge moved at contraction thresholds in skeletal muscle fibres. *J Physiol* **314**, 595–633.

Horowicz P & Schneider MF (1981*b*). Membrane charge movement in contracting and non-contracting skeletal muscle fibres. *J Physiol* **314**, 565–593.

Huang CL (1988). Intramembrane charge movements in skeletal muscle. *Physiol Rev* **68**, 1197–1147.

Hui CS (1983). Differential properties of two charge components in frog skeletal muscle. *J Physiol* **337**, 531–552.

Ikemoto N, Ronjat M, Meszaros LG & Koshita M (1989). Postulated role of calsequestrin in the regulation of calcium release from sarcoplasmic reticulum. *Biochemistry* **28**, 6764–6771.

Jayaraman T, Brillantes AM, Timerman AP, Fleischer S, Erdjument-Bromage H, Tempst P & Marks AR (1992). FK506 binding protein associated with the calcium release channel (ryanodine receptor). *J Biol Chem* **267**, 9474–9477.

Jong DS, Pape PC & Chandler WK (1995). Effect of sarcoplasmic reticulum calcium depletion on intramembranous charge movement in frog cut muscle fibres. *J Gen Physiol* **106**, 659–704.

Kovacs L, Rios E & Schneider MF (1979). Calcium transients and intramembrane charge movement in skeletal muscle fibres. *Nature* **279**, 391–396.

Lamb GD (1986*a*). Asymmetric charge movement in contracting muscle fibres in the rabbit. *J Physiol* **376**, 63–83.

Lamb GD (1986*b*). Components of charge movement in rabbit skeletal muscle: the effect of tetracaine and nifedipine. *J Physiol* **376**, 85–100.

Liu Y, Carroll SL, Klein MG & Schneider MF (1997). Calcium transients and calcium homeostasis in adult mouse fast-twitch skeletal muscle fibres in culture. *Am J Physiol Cell Physiol* **272**, C1919–1927.

Liu Y, Contreras M, Shen T, Randall WR & Schneider MF (2009). α-Adrenergic signalling activates protein kinase D and causes nuclear efflux of the transcriptional repressor HDAC5 in cultured adult mouse soleus skeletal muscle fibres. *J Physiol* **587**, 1101–1115.

Meissner G (1994). Ryanodine receptor/Ca^{2+} release channels and their regulation by endogenous effectors. *Annu Rev Physiol* **56**, 485–508.

Melzer W, Schneider MF, Simon BJ & Szucs G (1986). Intramembrane charge movement and calcium release in frog skeletal muscle. *J Physiol* **373**, 481–511.

Moore CP, Rodney G, Zhang JZ, Santacruz-Toloza L, Strasburg G & Hamilton SL (1999). Apocalmodulin and Ca^{2+} calmodulin bind to the same region on the skeletal muscle Ca^{2+} release channel. *Biochemistry* **38**, 8532–8537.

Most P, Remppis A, Weber C, Bernotat J, Ehlermann P, Pleger ST, Kirsch W, Weber M, Uttenweiler D, Smith GL, Katus HA, Fink RH (2003). The C terminus (amino acids 75–94) and the linker region (amino acids 42–54) of the Ca^{2+}-binding protein S100A1 differentially enhance sarcoplasmic Ca^{2+} release in murine skinned skeletal muscle fibres. *J Biol Chem* **278**, 26356–26364.

Most P, Remppis A, Pleger S, Katus H & Koch W (2007). S100A1: a novel inotropic regulator of cardiac performance. Transition from molecular physiology to pathophysiological relevance. *Am J Physiol Regul Integr Comp Physiol* **293**, R568–R577.

Nakai J, Dirksen RT, Nguyen HT, Pessah IN, Beam KG & Allen PD (1996). Enhanced dihydropyridine receptor channel activity in the presence of ryanodine receptor. *Nature* **380**, 72–75.

Nakai J, Sekiguchi N, Rando TA, Allen PD & Beam KG (1998). Two regions of the ryanodine receptor involved in coupling with L-type Ca^{2+} channels. *J Biol Chem* **273**, 13403–13406.

Pizarro G, Csernoch L, Uribe I, Rodríguez M & Ríos E (1991). The relationship between Q_γ and Ca release from the sarcoplasmic reticulum in skeletal muscle. *J Gen Physiol* **97**, 913–947.

Pizarro G, Fitts R, Uribe I & Ríos E (1989). The voltage sensor of excitation-contraction coupling in skeletal muscle. Ion dependence and selectivity. *J Gen Physiol* **94**, 405–428.

Pleger S, Most P, Boucher M, Soltys S, Chuprun J, Pleger W, Gao E, Dasgupta A, Rengo G, Remppis A, Katus H, Eckhart A, Rabinowitz J & Koch W (2007). Stable myocardial-specific AAV6-S100A1 gene therapy results in chronic functional heart failure rescue. *Circulation* **115**, 2506–2515.

Prosser B, Wright N, Hernandez-Ochoa E, Varney K, Liu Y, Olojo R, Zimmer D, Weber D & Schneider M (2007). S100A1 binds to the calmodulin-binding site of ryanodine receptor and modulates skeletal muscle excitation-contraction coupling. *J Biol Chem* **283**, 5046–5057.

Prosser B, Hernandez-Ochoa E, Zimmer D & Schneider M (2009). Simultaneous recording of intramembrane charge movement components and calcium release in wild-type and S100A$^{-/-}$ muscle fibres. *J Physiol* **587**, 4543–4559.

Protasi F, Paolini C, Nakai J, Beam KG, Franzini-Armstrong C & Allen PD (2002). Multiple regions of RyR1 mediate functional and structural interactions with α_{1S}-dihydropyridine receptors in skeletal muscle. *Biophys J* **83**, 3230–3244.

Reppel M, Sasse P, Piekorz R, Tang M, Roell W, Duan Y, Kletke A, Hescheler J, Nürnberg B & Fleischmann BK (2005). S100A1 enhances the L-type Ca^{2+} current in embryonic mouse and neonatal rat ventricular cardiomyocytes. *J Biol Chem* **280**, 36019–36028.

Ríos E & Pizarro G (1991). Voltage sensor of excitation-contraction coupling in skeletal muscle. *Physiol Rev* **71**, 849–908.

Rodney GG & Schneider MF (2003). Calmodulin modulates initiation but not termination of spontaneous Ca^{2+} sparks in frog skeletal muscle. *Biophys J* **85**, 921–932.

Royer L, Pouvreau S & Ríos E (2008). Evolution and modulation of intracellular calcium release during long-lasting, depleting depolarization in mouse muscle. *J Physiol* **586**, 4609–4629.

Schneider MF & Chandler WK (1973). Voltage dependent charge movement of skeletal muscle: a possible step in excitation-contraction coupling. *Nature* **242**, 244–246.

Schredelseker J, Dayal A, Schwerte T, Franzini-Armstrong C & Grabner M (2009). Proper restoration of excitation-contraction coupling in the dihydropyridine receptor β1-null zebrafish relaxed is an exclusive function of the β1a subunit. *J Biol Chem* **284**, 1242–1251.

Sencer S, Papineni RV, Halling DB, Pate P, Krol J, Zhang JZ & Hamilton SL (2001). Coupling of RYR1 and L-type calcium channels via calmodulin binding domains. *J Biol Chem* **276**, 38237–38241.

Simon BJ & Beam KG (1985). Slow charge movement in mammalian skeletal muscle. *J Gen Physiol* **85**, 1–19.

Tanabe T, Beam KG, Powell JA & Numa S (1988). Restoration of excitation-contraction coupling and slow calcium current in dysgenic muscle by dihydropyridine receptor complementary DNA. *Nature* **336**, 134–139.

Treves S, Scutari E, Robert M, Groh S, Ottolia M, Prestipino G, Ronjat M & Zorzato F (1997). Interaction of S100A1 with the Ca^{2+} release channel (ryanodine receptor) of skeletal muscle. *Biochemistry* **36**, 11496–11503.

Tripathy A, Xu L, Mann G & Meissner G (1995). Calmodulin activation and inhibition of skeletal muscle Ca^{2+} release channel (ryanodine receptor). *Biophys J* **69**, 106–119.

Tytgat J & Daenens P (1997). Effect of lanthanum on voltage-dependent gating of a cloned mammalian neuronal potassium channel. *Brain Res* **749**, 232–237.

Vinge LE, Raake PW & Koch WJ (2008). Gene therapy in heart failure. *Circ Res* **102**, 1458–1470.

Wang ZM, Messi ML & Delbono O (1999). Patch-clamp recording of charge movement, Ca^{2+} current, and Ca^{2+} transients in adult skeletal muscle fibres. *Biophys J* **77**, 2709–2716.

Wang ZM, Messi ML & Delbono O (2002). Sustained overexpression of IGF-1 prevents age-dependent decrease in charge movement and intracellular Ca^{2+} in mouse skeletal muscle. *Biophys J* **82**, 1338–1344.

Wright NT, Prosser BL, Varney KM, Zimmer DB, Schneider MF & Weber DJ (2008). S100A1 and calmodulin compete for the same binding site on ryanodine receptor. *J Biol Chem* **283**, 26676–26683.

Zimmer DB, Song W & Zimmer WE (1991). Isolation of a rat S100 α cDNA and distribution of its mRNA in rat tissues. *Brain Res Bull* **27**, 157–162.

Author contributions

B.L.P. performed the majority of experimentation, analysis, and writing involved with this work. E.O.H. contributed to all aspects of this work, particularly to experimental design and interpretation of results. D.B.Z. designed and provided the S100A1$^{-/-}$ animal and WT counterparts, and also critically revised and approved the final manuscript. M.F.S contributed to experimental design, analysis, and discussion. All the experiments presented above were performed in the lab of M.F.S., at the University of Maryland, Baltimore.

Acknowledgements

We would like to thank Drs Nathan Wright and David Weber for providing the Alexa labelled S100A1, as well as for insightful discussion stemming from their expertise with the S100 family of proteins. The project described was supported by grant no. RO1 QR055099 from the National Institute of Arthritis and Musculoskeletal and Skin Diseases. B.L.P. was supported by NIAMS training grant T32 AR007592 to the Interdisciplinary Program in Muscle Biology, University of Maryland School of Medicine.